

External forcing as a metronome for Atlantic multidecadal variability

Odd Helge Ottera^{1,2,3*}, Mats Bentsen^{1,2,3}, Helge Drange^{1,2,4} and Lingling Suo^{2,3}

Instrumental records, proxy data and climate modelling show that multidecadal variability is a dominant feature of North Atlantic sea-surface temperature variations^{1–4}, with potential impacts on regional climate⁵. To understand the observed variability and to gauge any potential for climate predictions it is essential to identify the physical mechanisms that lead to this variability, and to explore the spatial and temporal characteristics of multidecadal variability modes. Here we use a coupled ocean-atmosphere general circulation model to show that the phasing of the multidecadal fluctuations in the North Atlantic during the past 600 years is, to a large degree, governed by changes in the external solar and volcanic forcings. We find that volcanoes play a particularly important part in the phasing of the multidecadal variability through their direct influence on tropical sea-surface temperatures, on the leading mode of northern-hemisphere atmosphere circulation and on the Atlantic thermohaline circulation. We suggest that the implications of our findings for decadal climate prediction are twofold: because volcanic eruptions cannot be predicted a decade in advance, longer-term climate predictability may prove challenging, whereas the systematic post-eruption changes in ocean and atmosphere may hold promise for shorter-term climate prediction.

Coherent, large-scale sea-surface temperature (SST) variations are observed in the Atlantic Ocean on interannual to multidecadal timescales. A well-known, basin-wide variation is the Atlantic multidecadal oscillation (AMO), marked by alternation of warm and cold SST anomalies in the North Atlantic with a period of about 60–80 years⁶. Analysis of collections of multiple palaeo-proxies^{2,4} and tree-ring data⁷ indicates that AMO variability extends, at least, several centuries back in time. It has been suggested, on the basis of climate model simulations, that these variations are internally driven and related to multidecadal fluctuations in the Atlantic meridional overturning circulation (AMOC; refs 2,8,9). However, AMO is not solely driven by the changes in the AMOC, and attempts have been made to identify from observations the part of the signal that is linked to more global changes^{3,10,11}. If internal variability in the AMOC is the determining factor for the AMO, it suggests that it may be predictable¹². On the other hand, if external forcing agents such as total solar irradiance (TSI) variations and volcanic eruptions are important drivers, then these will have to be taken into account¹³. Identifying the relative role of internal variability and external forcing agents in driving multidecadal variability is therefore a key issue.

Here we use a fully coupled climate model, the Bergen climate model (BCM; ref. 14) (see Supplementary Section S1 for details), to demonstrate that external forcing has been instrumental in pacing the multidecadal variability in the Atlantic region over

the past 600 years. A total of seven simulations were carried out. In the first simulation, referred to as CTL600, the external forcing agents had no year-to-year variations and greenhouse-gas concentrations and tropospheric sulphate aerosols were fixed at pre-industrial (1850) levels. The second simulation, referred to as EXT600, included the external forcing due to changes in the amount of volcanic aerosols and variations in TSI for the past 600 years¹⁵ (Fig. 1a). The anthropogenic forcings were kept constant as in CTL600. Finally, five simulations covering the period 1850–1999 were run differing only by slight changes in the initial state. The ensemble mean of these simulations is referred to as ALL150. Here changes in tropospheric aerosols (Supplementary Fig. S1) and well-mixed greenhouse gases (Supplementary Fig. S2) were included in addition to the external forcing.

The simulated low-pass-filtered (see Methods) northern-hemisphere (NH) temperature back to 1400 (Fig. 1b, blue) generally falls within the spread of proxy-based NH temperature reconstructions (Fig. 1b, grey shading). Moreover, the simulated NH temperature in ALL150 (Fig. 1b, red) is highly correlated ($R = 0.9$) to the instrumental NH temperature¹⁶ (Fig. 1b, black). In EXT600 (Fig. 1b, blue) a relatively warm early-to-mid 20th century is found, with a general cooling over the past 40 years. The external forcing cannot therefore explain the late-20th-century warming¹⁷.

The observed AMO index for the past 150 years is characterized by warm phases in the late 19th century and from the 1930s to the 1960s, whereas cold phases occur during the first decades of the 20th century and from the mid-1960s to the 1980s (Fig. 1c, black). The simulated AMO in ALL150 is significantly correlated with the observations ($R = 0.68$) in terms of its phasing, but is too weak in amplitude (Fig. 1c, red and blue shading). However, the spread of the five ensemble members covers most of the variations in the observed AMO (Fig. 1c, grey shading). In contrast, the AMO in EXT600 shows no significant correlation to the observed AMO (Fig. 1c, blue). It should, however, be noted that for some periods the AMO in EXT600 follows the observed AMO closely, suggesting some role for the external forcing in pacing the AMO. On the other hand, the cold phase in the early 20th century is not seen in EXT600, but is evident in ALL150 (Fig. 1c). This points toward an anthropogenic origin for this signal. The observed spatial pattern of the AMO since 1850 (Fig. 1d) has some similarities to the one simulated in ALL150 (Fig. 1e), in particular in the northern North Atlantic and off the west coast of Africa.

The simulated AMO and AMOC indices for EXT600 are shown in Fig. 2a together with reconstructed AMO indices based on multiproxy⁴ (Fig. 2a, dark green) and tree-ring⁷ (Fig. 2a, light green) data. The correlations between the simulated and reconstructed AMO indices are positive (multiproxy $R = 0.24$; tree-ring $R = 0.26$), but barely significant. However, strong covariations

¹Uni Bjerknæs Center, Allégaten 55, N-5007 Bergen, Norway, ²Bjerknæs Center for Climate Research, Allégaten 55, N-5007 Bergen, Norway, ³Nansen Environmental and Remote Sensing Center, Thormøhlensgate 47, N-5006 Bergen, Norway, ⁴Geophysical Institute, University of Bergen, Allégaten 70, N-5007 Bergen, Norway. *e-mail: Odd.Ottera@uni.no.

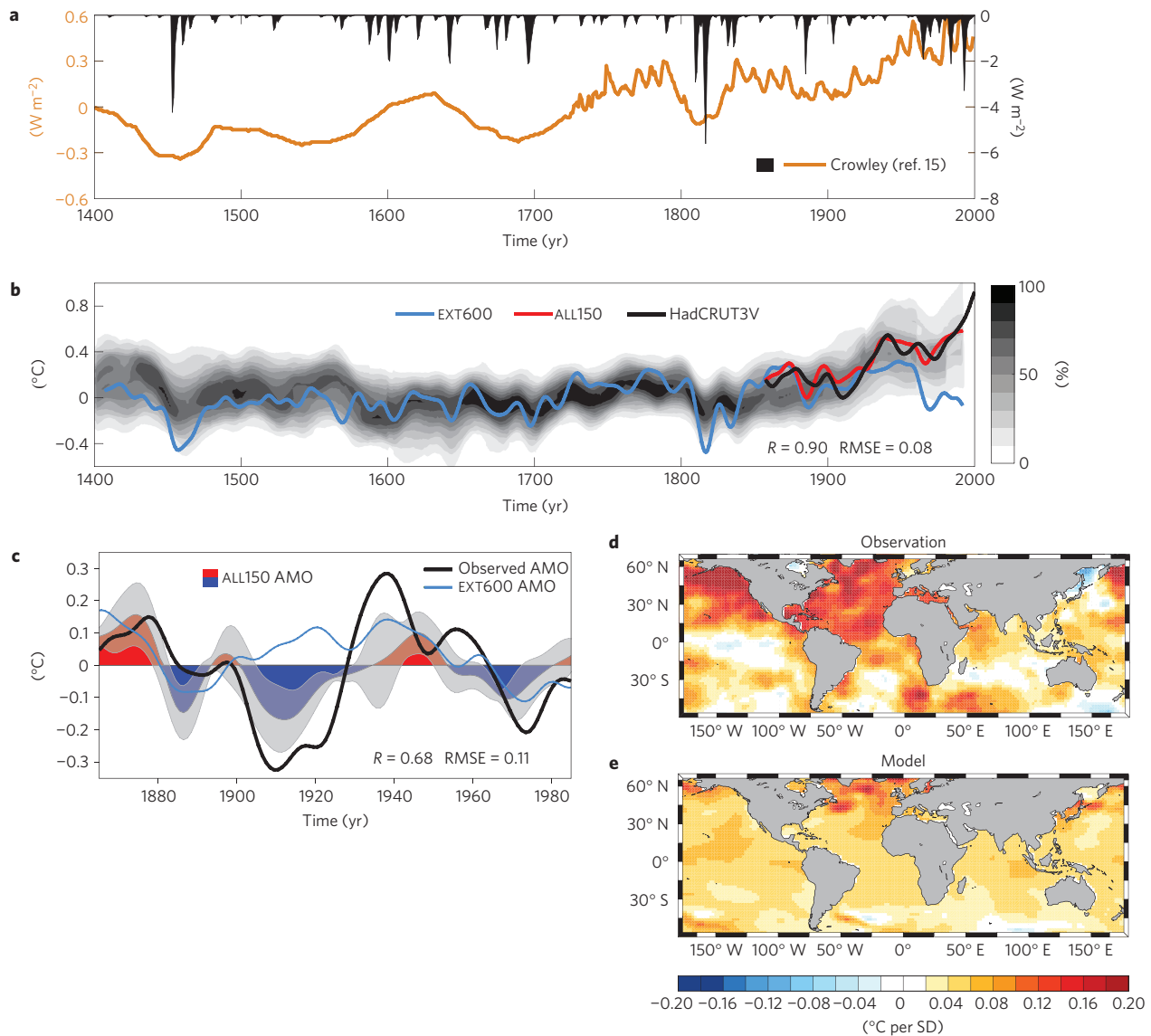


Figure 1 | Observed and simulated northern hemisphere temperature and Atlantic multidecadal oscillation. a, Volcanic and TSI forcings¹⁵. **b**, Observed (ref. 16, black) and simulated NH surface-air-temperature anomalies in EXT600 (blue) and ALL150 (red) together with the concentration of overlapping NH temperature reconstructions (ref. 17, shading). **c**, AMO indices for the past 150 years for observations (black), EXT600 (blue) and ALL150 (red and blue shading). The grey shaded region represents the standard deviation of the individual ensemble members. **d**, Observed spatial pattern obtained by regressing the detrended and low-pass-filtered SST data on a standardized version of the AMO index. **e**, The same as **d**, but for ALL150. Correlations ($\alpha < 0.1$) and root mean square errors between ALL150 and observations are shown in **b** and **c**.

between the AMO indices are found for some periods, notably during the cold periods in the late 17th and early 19th centuries.

Geographical patterns of decadal-to-multidecadal variability at the ocean surface in EXT600 are illustrated by empirical orthogonal functions (EOFs) of low-pass-filtered global SSTs (ref. 3). In Fig. 2b,c we show the first and third EOFs. The associated first and third principal components (PCs) show significant positive correlations to the external forcing and the AMOC, respectively (Fig. 2d–f). The second EOF and its associated PC reflect model drift during the first few centuries of the model integrations¹⁴ and are not shown. The first EOF is characterized by large positive anomalies in the tropical North Atlantic, and weaker or even negative anomalies in the sub-polar region (Fig. 2b). The associated PC1 (Fig. 2a, grey) is strongly correlated to the AMO index ($R = 0.8$), indicating a causal link between the external forcing and the AMO.

The third EOF is characterized by large positive anomalies in the sub-polar region and small positive or slightly negative

anomalies in the tropical North Atlantic (Fig. 2c). As the associated PC3 is positively correlated to the AMOC (Fig. 2a,f, pink), this suggests that AMOC influence is mostly restricted to the sub-polar region in EXT600. Interestingly, the corresponding EOF in CTL600 is characterized by a dipole structure in the Atlantic, with basin-wide positive anomalies in the North Atlantic and negative anomalies in the South Atlantic (Supplementary Fig. S3). The latter is significantly correlated to the AMOC, with the AMOC leading by about 5–10 years, suggesting a key role for the AMOC in setting the basin-wide Atlantic SSTs in CTL600 (refs 2,8,9).

Positive TSI anomalies lead, through radiative forcing, to an SST increase in the North Atlantic that tends to weaken the AMOC (refs 18,19), in line with the projected response under global-warming conditions²⁰. In EXT600, such an effect is found with negative (but not significant) correlations between the TSI forcing and the AMOC, with about 10 years lag (Fig. 2d, purple). However, the negative correlations for the total forcing are larger

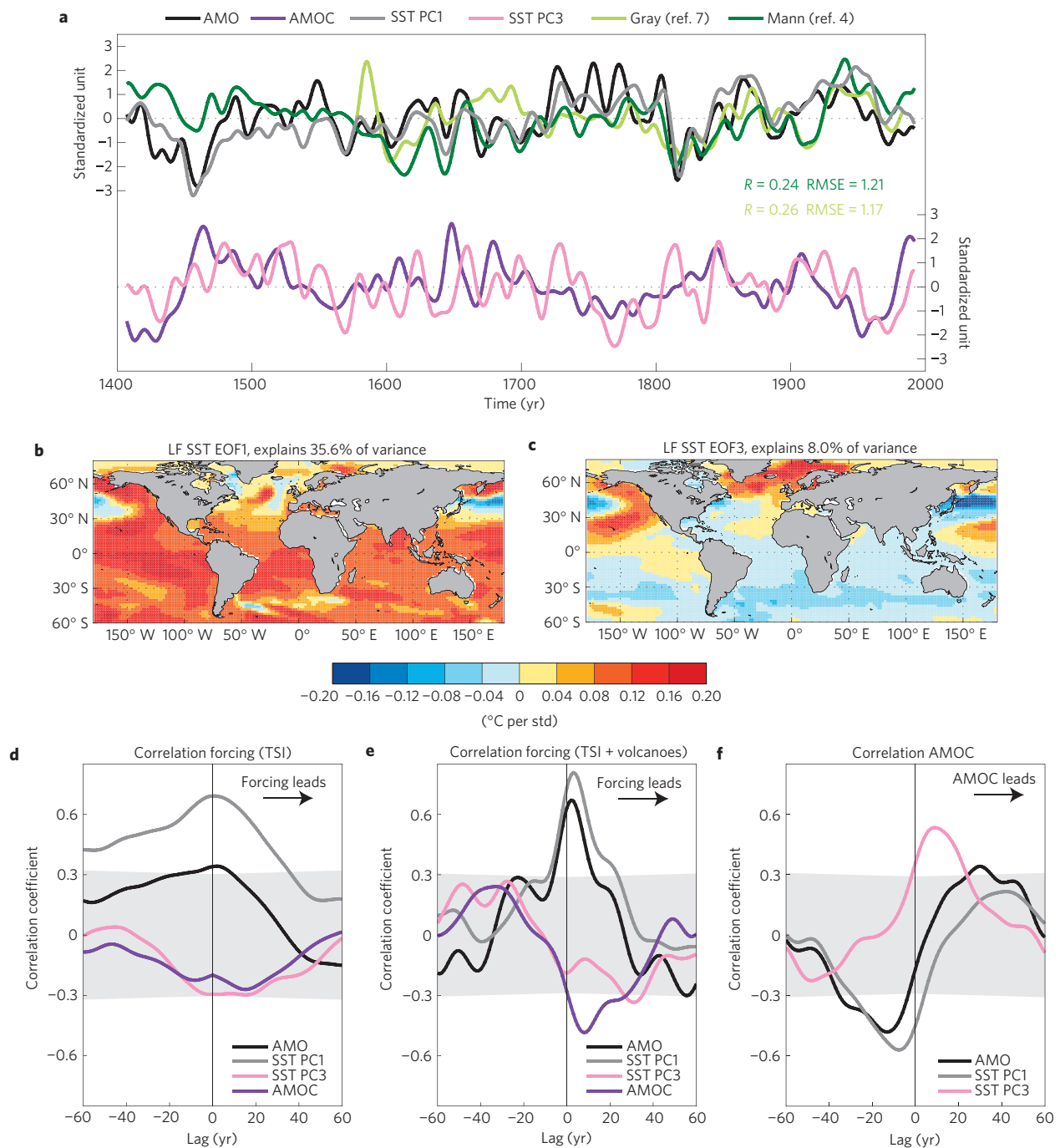


Figure 2 | The role of external forcing for Atlantic multidecadal variability. **a**, Simulated standardized indices of AMO (black), AMOC (purple), global SST PC1 (grey) and PC3 (pink) together with reconstructed standardized AMO indices based on multiple proxies (ref. 4, dark green) and tree-ring data (ref. 7, light green). Correlations ($\alpha < 0.1$) and root mean square errors between EXT600 and reconstructions are also shown. **b**, Regression of global SST in EXT600 on PC1. **c**, The same as **b**, but for PC3. **d**, Cross-correlations of the simulated AMO, PC1, PC3 and AMOC indices with the TSI forcing in EXT600. Positive lags mean that the forcing is leading. **e**, The same as **d**, but for correlations with the total (TSI + volcano) forcing. **f**, Cross-correlations of the simulated AMO, PC1 and PC3 indices with the AMOC index. Positive lags mean that the AMOC is leading. In **d–f** significance levels ($\alpha < 0.05$) are shown in grey shading.

and significant (Fig. 2e, purple), suggesting an important role for volcanoes in AMOC.

Also, significant negative correlations are found between the AMO and the AMOC, with the AMO leading by about 10 years (Fig. 2f, black). This is due to the fact that basin-wide Atlantic SSTs, as reflected in the AMO index, are dominated by the much larger (area-averaged) tropical North Atlantic region, which is largely controlled by external forcing in EXT600. This implies that the

AMOC reaches its minimum (maximum) values about 10 years after the AMO reaches its highest (lowest) values. Consequently, there is no one-to-one relationship between the AMOC and the AMO in EXT600, in contrast to CTL600.

The impact of the winter North Atlantic oscillation (NAO; ref. 21) on the North Atlantic Ocean, and notably on the AMOC, has been extensively discussed in the literature^{22,23}. The general ocean response to interannual NAO variability in the BCM

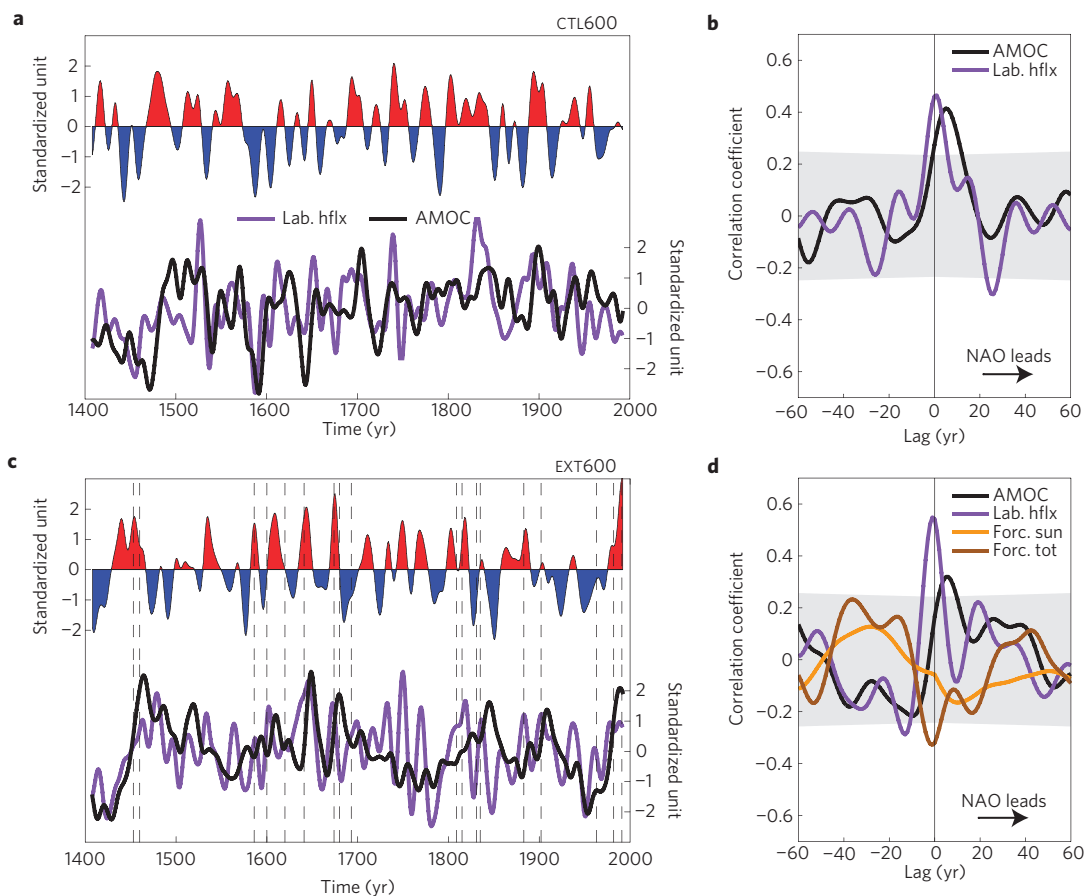


Figure 3 | Simulated North Atlantic oscillation and Atlantic meridional overturning circulation. **a**, Simulated standardized NAO (red and blue shading), AMOC (black) and Labrador Sea heat-flux (purple; positive values indicate flux to the atmosphere) indices in CTL600. **b**, Cross-correlations of the NAO index with the AMOC and Labrador Sea heat-flux indices for CTL600. The grey-shaded region represents the significance levels ($\alpha < 0.05$). Positive lags means that the NAO is leading. **c**, The same as **a**, but for EXT600. Large tropical eruptions are indicated with dashed lines. **d**, The same as **b**, but for EXT600. The cross-correlations of the NAO index with the solar- and total-external-forcing time series are also shown.

compares favourably to observations (Supplementary Section S2). In the following we focus on the role of the atmospheric circulation in modulating the multidecadal AMOC variations in the BCM. The simulated NAO and AMOC indices for CTL600 and EXT600 are shown in Fig. 3a,c. In both simulations we find significant correlations between the NAO and the AMOC indices, with the NAO leading the AMOC by 5–10 years (Fig. 3b,d). There is also, in general, a significant dominant response of the heat- and momentum-flux variations in the Labrador Sea as part of the NAO (Fig. 3 and Supplementary Fig. S4). In the model, the strength of the AMOC is largely controlled by the formation of intermediate and deep waters in the Labrador Sea region (Supplementary Section S3 and Fig. S5). Our results thus suggest that interdecadal variations in the NAO, through its dominant buoyancy forcing in the Labrador Sea, play an important role in the phasing of the multidecadal variability of the AMOC.

Previous studies have suggested lagged relationships between low-frequency TSI variations and the NAO (refs 19,24). The proposed mechanisms involve atmospheric teleconnections from the Pacific Ocean¹⁹ as well as stratosphere–troposphere coupling²⁴. In EXT600, we find no significant correlation between the simulated NAO and the applied TSI forcing (Fig. 3d, orange). However, there is a significant negative correlation between the NAO and the total external forcing, suggesting a potential role for volcanoes. In EXT600, positive or increasing NAO is typically associated with large tropical volcanic eruptions (Fig. 3c,

dashed lines). It is known from both observations and other modelling studies that large tropical eruptions have a tendency to induce a positive NAO response, causing the well-known posteruption winter warming phenomenon over NH land masses^{25,26}. However, climate models have only shown limited ability in simulating this robust, observation-based feature²⁷, possibly linked to inadequate treatment of stratosphere–troposphere dynamical interactions.

In EXT600, the volcanic aerosols are injected directly into the stratosphere, where they can modify both the short-wave and long-wave radiation²⁶. Because of this, the volcanic eruptions lead to strong heating of the lower tropical stratosphere by absorption of terrestrial and solar near-infrared radiation (Fig. 4a). This layer is then expanded, producing an enhanced pole-to-equator temperature difference, also increasing the geopotential height gradient (Fig. 4b, red). The strengthened polar vortex that follows (Fig. 4b, blue) traps the wave energy of the tropospheric circulation, and the NAO dominates the winter circulation (Fig. 4c), producing winter warming over large parts of the NH land masses (Fig. 4d). We also find a strong response in the total heat flux in the Labrador Sea after large eruptions, tending to increase the local buoyancy forcing and subsequently speed up the AMOC a few years after the eruption (Fig. 4e). An important result from this study is therefore that explosive volcanism has a strong influence on NH climate, not only for short-term changes, but also for multidecadal AMO-type changes. Volcanic eruptions tend to strengthen the AMOC through their direct radiative cooling²⁸,

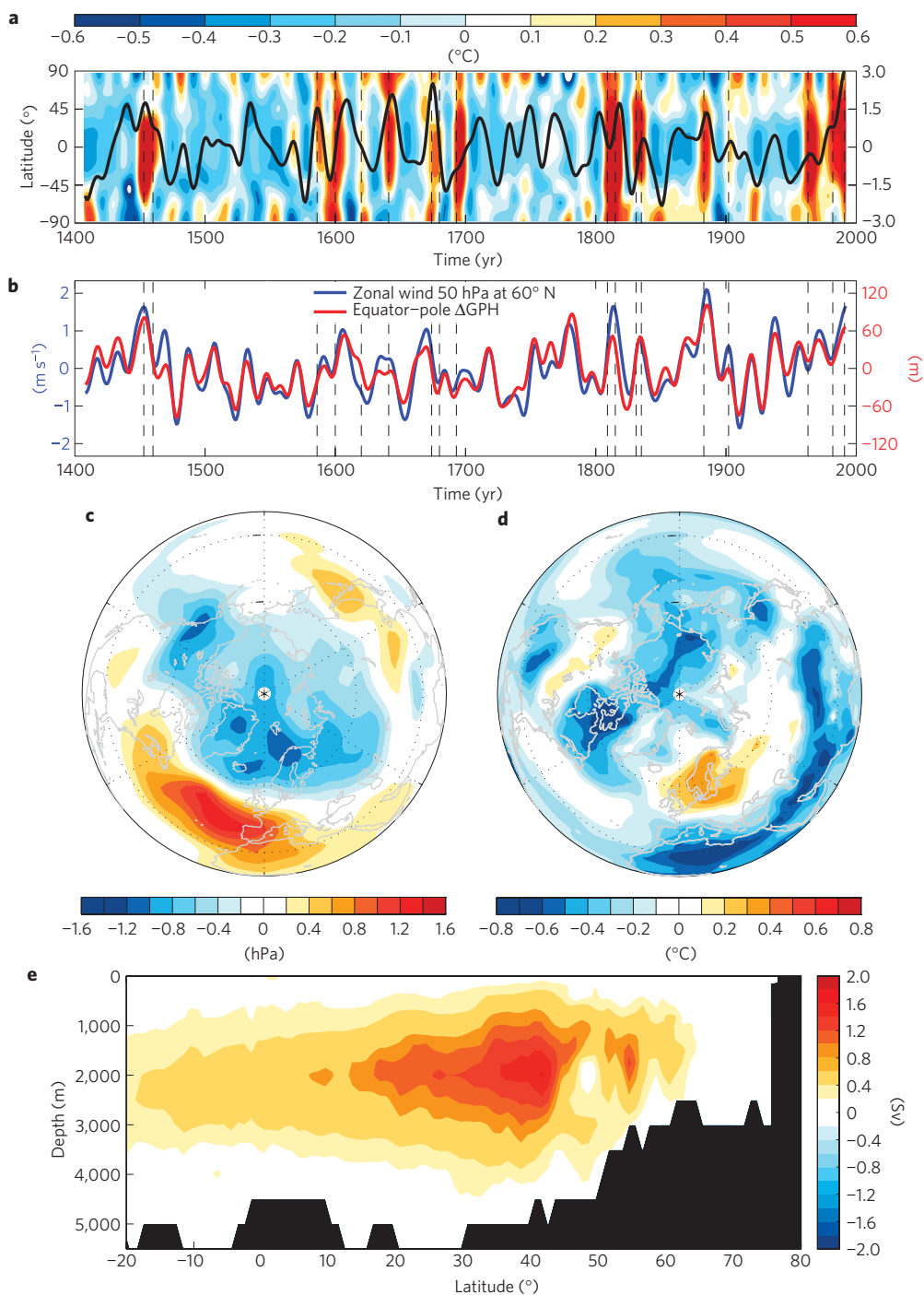


Figure 4 | Simulated responses to volcanic forcing. **a**, Simulated annual mean lower-stratospheric (50 hPa) temperature anomalies (contours) and simulated NAO (black) in EXT600. **b**, Simulated lower-stratospheric (50 hPa) winter (December–February) zonal wind strength at 60° N (blue) and equator-to-pole gradient in geopotential height (Δ GPH, red). Large tropical eruptions are indicated with dashed lines. **c**, Composite analysis showing the mean NH winter sea-level pressure anomalies in the two winters following large tropical eruptions in EXT600. **d**, The same as **c**, but for surface air temperature. **e**, The same as **c**, but for the Atlantic meridional streamfunction, averaged over years 5–10 following the volcanic eruption.

and in the BCM also through their tendency to induce positive phases of the NAO.

There are possible caveats to the presented findings. For example, it could be argued that the BCM underestimates the internal variability of the AMOC on multidecadal timescales. This question is, however, difficult to adequately address in the absence of instrumental observations of the AMOC. Furthermore, the TSI reconstruction used here is in the upper end of recent estimates¹⁷. Further sensitivity studies, with different TSI reconstructions,

are therefore necessary to clarify the role of this forcing in Atlantic SST variability.

Although the external forcing is clearly important for the AMO characteristics in the BCM (Supplementary Section S4 and Fig. S6), it cannot explain all of the simulated variability. In the model, and also probably in nature, there is an interplay between the intrinsic climate variability and the external forcing. Rather, we conclude that the external forcing acts as a metronome for the Atlantic multidecadal variability. In view of this, the frequency and intensity

of external forcing need to be better understood and quantified to produce reliable near-term climate forecasts.

Methods

Forcings. The TSI forcing¹⁵ is incorporated as variations in the effective solar constant in the BCM. This modifies the top of the atmospheric short-wave flux in EXT600 and ALL150. The volcanic aerosol forcing¹⁵ includes the monthly optical depths at 0.55 μm in the middle of the visible spectrum in four bands (90° N–30° N, 30° N–equator, equator–30° S and 30° S–90° S). The aerosol loading was distributed in each model level in the stratosphere using a weighting function²⁶. The volcanic mass of the stratospheric aerosols was then calculated at each grid-point and model level in the stratosphere by dividing the total aerosol concentration by the total air mass of all stratospheric levels at that grid point. In Fig. 1a the original aerosol loading values have been converted to radiative forcing by dividing by 30 and multiplying by 23.5 (ref. 29). The changes in well-mixed greenhouse gas concentrations and tropospheric aerosols are taken from the forcing data set prepared for the EU project ENSEMBLES. Details of the forcing data can be found at <http://www.cnrm.meteo.fr/ensembles/public/results/results.html>.

Definition of indices. The simulated and reconstructed NH surface-air-temperature anomalies are calculated with respect to a 1500–1899 reference period. The observed NH temperature anomalies¹⁶ are given with respect to a 1961–1990 reference period, but adjusted here by +0.45 °C so that they have the same 1881–1990 mean as ALL150. The observed and simulated AMO indices were defined as the annual mean SST averaged over the region 0° N–60° N, 75° W–7.5° W. The observed AMO index is calculated on the basis of the National Oceanic and Atmospheric Administration extended reconstructed SST data set³⁰. The AMO indices calculated from observations and ALL150 have been linearly detrended. A common diagnostic for the strength of the Atlantic thermohaline circulation is the maximum strength of the AMOC. In this study we define the AMOC index as the maximum of the Atlantic streamfunction between 20° N and 50° N. Alternative formulations, such as the maximum of the Atlantic streamfunction at 30° N or the leading PC of the overturning stream function, yield very similar results (not shown). The NAO indices for CTL600 and EXT600 are defined as the first PC of winter mean sea-level pressure (December–February) for all points north of 20° N. The corresponding spatial patterns are shown in Supplementary Fig. S7. The Labrador Sea heat-flux indices are calculated by averaging over the Labrador Sea mixing region (Supplementary Fig. S5) and over the extended winter season (November–April). The lower-stratosphere geopotential height gradient is estimated by calculating a linear least-square fit to the zonal-mean geopotential height, and then calculating the equator-to-pole (0° N–90° N) difference.

Ensemble initialization technique. In ALL150, perturbations to the initial conditions were made using the common method of taking different atmospheric, but identical ocean, start conditions for the model¹². In our case the different atmospheric initial conditions were generated from a previous 20 day simulation using a daily restart file every five days. This perturbation methodology is in no way optimal in terms of, for example, sampling the likely range of subdecadal atmosphere–ocean analysis error. However, it is sufficient to generate ensemble spread on the timescales of interest here.

Composite analysis. Before the composite analysis shown in Fig. 4, objective criteria were used to select the largest eruptions from the volcanic-forcing data set. The criteria were years for which the estimated negative global radiative forcing from the volcanic eruption exceeded 1 W m⁻², and the rate of change of the forcing (that is forcing in year n minus that in year $n - 1$) was greater than 0.5 W m⁻². A total of 18 eruptions over the past 600 years pass these criteria and are listed in Supplementary Table S1. The eruptions are also marked as dashed lines in Figs 3c and 4a,b.

Statistical methods. The focus of this study has been on the low-frequency (multidecadal) variability. Therefore, a third-order Butterworth filter with cut-off frequency of 15 years has been used to filter all data. Standard linear regression has been used to calculate regression maps, whereas EOFs have been calculated using standard singular-value decomposition analysis. Furthermore, the Singular Spectrum Analysis—Multitaper Method (SSA-MTM) Toolkit has been used to calculate the power spectra in Supplementary Fig. S6. The toolkit and its documentation can be downloaded from <http://www.atmos.ucla.edu/tcd/ssa/>. Finally, lagged correlations have been made from low-pass-filtered time series. Significance levels were calculated using a standard t test. Autocorrelation is taken into account by adjusting the effective number of independent observations.

Received 1 March 2010; accepted 10 August 2010; published online 12 September 2010

References

- Folland, C. K., Parker, D. E. & Palmer, T. N. Sahel rainfall and worldwide sea temperatures, 1901–85. *Nature* **320**, 602–607 (1986).
- Delworth, T. L. & Mann, M. E. Observed and simulated multi-decadal variability in the Northern Hemisphere. *Clim. Dyn.* **16**, 661–676 (2000).
- Parker, D. *et al.* Decadal to multidecadal variability and the climate change background. *J. Geophys. Res.* **112**, D18115 (2007).
- Mann, M. E. *et al.* Global signatures and dynamical origins of the little ice age and medieval climate anomaly. *Science* **326**, 1256–1260 (2009).
- Knight, J. R., Folland, C. K. & Scaife, A. Climate impacts of the Atlantic Multidecadal Oscillation. *Geophys. Res. Lett.* **33**, L17706 (2006).
- Schlesinger, M. E. & Ramankutty, N. An oscillation in the global climate system of period 65–70 years. *Nature* **367**, 723–726 (1994).
- Gray, S. T., Graumlich, L. J., Betancourt, J. L. & Pederson, G. T. A tree-ring based reconstruction of the Atlantic multidecadal oscillation since 1567 A.D. *Geophys. Res. Lett.* **31**, L12205 (2004).
- Jungclauss, J., Haak, H., Latif, M. & Mikolajewicz, U. Arctic–North Atlantic interactions and multidecadal variability of the meridional overturning circulation. *J. Clim.* **18**, 4013–4031 (2005).
- Knight, J. R., Allan, R. J., Folland, C. K., Vellinga, M. & Mann, M. E. A signature of persistent natural thermohaline circulation cycles in observed climate. *Geophys. Res. Lett.* **32**, L20708 (2005).
- Trenberth, K. E. & Shea, D. J. Atlantic hurricanes and natural variability in 2005. *Geophys. Res. Lett.* **33**, L12704 (2006).
- Guan, B. & Nigam, S. Analysis of Atlantic SST variability factoring interbasin links and the secular trend: Clarified structure of the Atlantic multidecadal oscillation. *J. Clim.* **22**, 4228–4240 (2009).
- Collins, M. *et al.* Interannual to decadal predictability in the North Atlantic: A multimodel-ensemble study. *J. Clim.* **19**, 1195–1203 (2006).
- Lean, J. L. & Rind, D. How will Earth's surface temperature change in future decades? *Geophys. Res. Lett.* **36**, L15708 (2009).
- Otterå, O. H., Bentsen, M., Bethke, I. & Kvamstø, N. G. Simulated pre-industrial climate in Bergen climate model (version 2): Model description and large-scale circulation features. *Geosci. Mod. Dev.* **2**, 197–212 (2009).
- Crowley, T. J., Baum, S. K., Kim, K.-Y., Hegerl, G. C. & Hyde, W. T. Modeling ocean heat content changes during the last millennium. *Geophys. Res. Lett.* **30**, 1932 (2003).
- Brohan, P., Kennedy, J. J., Harris, I., Tett, S. F. B. & Jones, P. D. Uncertainty estimates in regional and global observed temperature changes: A new dataset from 1850. *J. Geophys. Res.* **111**, D12106 (2006).
- Jansen, E. *et al.* in *IPCC WG1 Fourth Assessment Report* (eds Solomon, S. *et al.*) (Cambridge Univ. Press, 2007).
- Latif, M., Park, W., Ding, H. & Keenlyside, N. S. Internal and external North Atlantic sector variability in the Kiel climate model. *Meteorol. Zeit.* **18**, 433–443 (2009).
- Swingedouw, D. *et al.* Natural forcing of climate during the last millennium: Fingerprint of solar variability. *Clim. Dyn.* (doi:10.1007/s00382-010-0803-5) (2010, in the press).
- Gregory, J. M. *et al.* A model intercomparison of changes in the Atlantic thermohaline circulation in response to increasing atmospheric CO₂ concentration. *Geophys. Res. Lett.* **32**, L12703 (2005).
- Hurrell, J. W. Decadal trends in the North Atlantic oscillation: Regional temperatures and precipitation. *Science* **269**, 676–679 (1995).
- Eden, C. & Jung, T. North Atlantic interdecadal variability: Oceanic response to the North Atlantic oscillation (1865–1997). *J. Clim.* **14**, 676–691 (2001).
- Delworth, T. L. & Greatbatch, R. J. Multidecadal thermohaline circulation variability driven by atmospheric surface flux forcing. *J. Clim.* **13**, 1481–1495 (2000).
- Shindell, D. T., Schmidt, G. A., Mann, M. E., Rind, D. & Waple, A. Solar forcing of regional climate change during the Maunder minimum. *Science* **294**, 2149–2155 (2001).
- Robock, A. Volcanic eruptions and climate. *Rev. Geophys.* **38**, 191–219 (2000).
- Otterå, O. H. Simulating the effects of the 1991 Mount Pinatubo volcanic eruption using the ARPEGE atmosphere general circulation model. *Adv. Atmos. Sci.* **25**, 213–226 (2008).
- Stenchikov, G. *et al.* Climate impacts of volcanic eruptions in the IPCC AR4 climate models. *J. Geophys. Res.* **111**, D07107 (2006).
- Stenchikov, G. *et al.* Volcanic signals in oceans. *J. Geophys. Res.* **114**, D16104 (2009).
- Sato, M., Hansen, J. E., McCormick, M. P. & Pollack, J. B. Stratospheric aerosol optical depths 1850–1990. *J. Geophys. Res.* **98**, 22987–22994 (1993).
- Smith, T. M., Reynolds, R. W., Peterson, T. C. & Lawrimore, J. Improvements to NOAA's historical merged land–ocean surface temperature analysis (1880–2006). *J. Clim.* **21**, 2283–2296 (2008).

Acknowledgements

We thank M. Miles, T. Eldevik and T. Furevik for comments on an earlier version of the manuscript. This study has been supported by the Research Council of Norway through the NorClim and ARCWARM projects, and by the Program of Supercomputing. Financial support by the EU FP6 Integrated Project ENSEMBLES (Contract 505539) is

acknowledged. This study also contributes to the EU FP6 integrated project THOR, and the DecCen project financed by the Research Council of Norway. This is Publication A296 from the Bjerknæs Centre for Climate Research.

Author contributions

O.H.O. conceived the study, designed the model experiments and wrote the initial manuscript. O.H.O., M.B. and L.S. carried out the BCM experiments. O.H.O. processed the model results and did the main analyses. H.D. contributed to the scientific results

through discussions and analyses. All authors participated in writing the paper and analysing the results.

Additional information

The authors declare no competing financial interests. Supplementary information accompanies this paper on www.nature.com/naturegeoscience. Reprints and permissions information is available online at <http://npg.nature.com/reprintsandpermissions>. Correspondence and requests for materials should be addressed to O.H.O.